A&A 463, 481–492 (2007)
DOI: 10.1051/0004-6361:20054146

Astronomy & Astrophysics

Galactic star formation rates gauged by stellar end-products

M. Persic[1] and Y. Rephaeli[2,3]

[1] INAF/Osservatorio Astronomico di Trieste, via G.B. Tiepolo 11, 34143 Trieste, Italy
e-mail: persic@oats.inaf.it
[2] School of Physics and Astronomy, Tel Aviv University, Tel Aviv 69978, Israel
[3] CASS, University of California, San Diego, La Jolla, CA 92093, USA

Received 5 September 2005 / Accepted 12 October 2006

ABSTRACT

Young galactic X-ray point sources (XPs) closely trace the ongoing star formation in galaxies. From measured XP number counts we extract the collective 2−10 keV luminosity of young XPs, $L_{\rm x}^{\rm yXP}$, which we use to gauge the current star formation rate (SFR) in galaxies. We find that, for a sample of local star-forming galaxies (i.e., normal spirals and mild starbursts), $L_{\rm x}^{\rm yXP}$ correlates linearly with the SFR over three decades in luminosity. A separate, high-SFR sample of starburst ULIRGs can be used to check the calibration of the relation. Using their (presumably SF-related) total 2−10 keV luminosities we find that these sources satisfy the SFR–$L_{\rm x}^{\rm yXP}$ relation, as defined by the weaker sample, and extend it to span ∼5 decades in luminosity. The SFR–$L_{\rm x}^{\rm yXP}$ relation is also likely to hold for distant ($z \sim 1$) *Hubble* Deep Field North galaxies, especially so if these high-SFR objects are similar to the (more nearby) ULIRGs. It is argued that the SFR–$L_{\rm x}^{\rm yXP}$ relation provides the most adequate X-ray estimator of instantaneous SFR by the phenomena characterizing massive stars from their birth (FIR emission from placental dust clouds) through their death as compact remnants (emitting X-rays by accreting from a close donor). For local, low/intermediate-SFR galaxies, the simultaneous existence of a correlation of the instantaneous SFR with the total 2−10 keV luminosity, $L_{\rm x}$, which traces the SFR integrated over the last $\sim 10^9$ yr, suggests that during such epoch the SF in these galaxies has been proceeding at a relatively constant rate.

Key words. galaxies: starburst – infrared: galaxies – radio continuum: galaxies – X-rays: binaries – X-rays: galaxies

1. Introduction

Star formation (SF) leads to X-ray emission on various spatial and temporal scales, including emission from O stars, X-ray binaries, supernovae (SN) and their remnants (SNRs), galactic-scale emission from diffuse hot gas, and Compton scattering of FIR & CMB photons by SN-accelerated electrons. Integrated spectra of star-forming galaxies (SFGs) are expected to show all these components, as well as emission from an active nucleus (Rephaeli et al. 1991, 1995). Based on lower-resolution X-ray data (mainly from *Einstein*, *ASCA*, *BeppoSAX*, and *RXTE*), most SFGs have remarkably similar integrated spectra that include a soft (single- or multiple-temperature) sub-keV thermal component that dominates at energies $\epsilon \lesssim 2$ keV, plus a hard power law (PL) that dominates at $\epsilon \gtrsim 2$ keV (e.g., Dahlem et al. 1998). By quantitatively assessing the spectral components of the various X-ray emission mechanisms in SFGs, Persic & Rephaeli (2002) concluded that the 2−10 keV emission is dominated by compact X-ray binaries, specifically HMXBs if the star formation rate (SFR) is very high.

Stellar-related X-ray emission can be used as an indicator of SFR (David et al. 1992; Bauer et al. 2002; Grimm et al. 2003; Franceschini et al. 2003; Ranalli et al. 2003; Gilfanov et al. 2004a). The basic notion is that the ongoing SFR can be measured based on stellar end-products that are both sufficiently X-ray-bright for their collective emission to be unambiguously identified, and sufficiently short-lived so that they trace the "instantaneous" SFR. Of the three main types of Galactic stellar endproduct X-ray sources (LMXBs, SNRs, and HMXBs), the latter two provide a suitable combination of short delay between star formation and onset of X-ray emission and significant X-ray brightness.

Persic et al. (2004a) examined ways in which the 2−10 keV luminosity (hereafter: $L_{\rm x}$) can be used as an estimator of ongoing galactic SFR. They concluded that the collective 2−10 keV emission from HMXBs, $L_{\rm x}^{\rm HMXB}$, was a reliable SFR estimator (supporting independent suggestions by, e.g., Grimm et al. 2003). Given the diverse sources of X-ray emission in SFGs, Persic et al. (2004a) argued that the level of HMXB emission could be evaluated by modeling SFG spectra with Persic & Rephaeli's (2002) template – in which the HMXB component was represented as a $\Gamma = 1.2$ power law. Upon analyzing suitable *ASCA*, *BeppoSAX*, and *Newton/XMM* spectra, Persic et al. (2004a) suggested that $L_{\rm x}^{\rm HMXB} \sim 0.2\,L_{\rm x}$ in moderately star-forming galaxies and $L_{\rm x}^{\rm HMXB} \sim L_{\rm x}$ in intensely star-forming ones.

However, Persic et al.'s (2004a) approach was potentially limited. The template SFG spectrum of Persic & Rephaeli (2002), on which their spectral analysis was based, explicitly assumed a Galactic stellar population: in principle that feature could bias Persic et al.'s (2004a) procedure because any SF-tracing population of X-ray point sources (XPs), not represented in our own Galaxy but present elsewhere (and spectrally different from Galactic HMXBs), would be missed. This actually turns out to be the case for the Ultra-Luminous X-ray sources (ULXs) that dominate the XP luminosity ($L_{\rm XP}$) of most SFGs. Furthermore, few integrated spectra were of sufficiently good quality to be fitted with the multi-component template of Persic & Rephaeli (2002).

It is important then to further scrutinize the role and effectiveness of the collective 2−10 keV emission of young XPs, $L_{\rm x}^{\rm yXP}$, in measuring the ongoing SFR in galaxies – as well as ways to evaluate it. In this paper we propose to evaluate $L_{\rm x}^{\rm yXP}$ by modeling the luminosity functions of galactic XPs (hereafter: XPLFs) as linear combinations of the "universal" young- and old-XPLFs. To demostrate the effectiveness of the proposed technique, we will apply it to a sample of galaxies with available *Chandra* XPLFs. For the same sample, we will then check how the derived values of $L_{\rm x}^{\rm yXP}$ correlate with the ongoing SFR as deduced from the galaxies' (thermal) FIR and (non-thermal) radio emission.

The plan of this paper is as follows. In Sect. 2 we review the properties of XPLFs in galaxies. The two local and nearby samples of star-forming galaxies are described in Sect. 3. In Sect. 4 we review the FIR- and radio-based SFR indicators. In Sect. 5 we apply our proposed young/old-XP decomposition technique to a sample of SFGs and evaluate $L_{\rm x}^{\rm yXP}$, which are then contrasted with FIR/radio-based SFRs: the results are discussed in Sect. 6. In Sect. 7 we extend our investigation to high-SFR galaxies, and discuss SF in the nearby universe. In Sect. 8 we discuss X-ray SFR indicators at high redshift. X-ray and radio SFR indicators are compared in Sect. 9. Section 10 closes with a short summary of our main results. Throughout this paper we assume $\Omega_0 = 1$, $H_0 = 75\ {\rm km\,s^{-1}\,Mpc^{-1}}$. (No result in this paper is substantially affected by choosing this one particular cosmology.)

2. X-ray point sources in galaxies

Observations of nearby galaxies led to the detection of XPs and their luminosity functions (XPLFs) down to limiting luminosities of $\sim 10^{36}\ {\rm erg\,s^{-1}}$ (see Fabbiano 2006 for a recent comprehensive review.) Such XPs include SNRs, close binary systems in which the accreting object can be either a pulsar ($L_{\rm x} \leq 2\times 10^{38}\ {\rm erg\,s^{-1}}$) or a black hole (BH) ($2\times 10^{38} \leq L_{\rm x}/({\rm erg\,s^{-1}}) \leq 10^{39}$), and ULXs ($L_{\rm x} > 10^{39}\ {\rm erg\,s^{-1}}$). The quoted limits correspond to Eddington luminosities for spherical accretion onto $\sim 2\,M_\odot$ and $\sim 8\,M_\odot$ BHs, respectively, which is the approximate range of BH masses that are thought to be attainable via ordinary stellar evolution.

Young SNRs, which result from the explosion of short-lived $\gtrsim 5\ M_\odot$ progenitor stars and are X-ray bright for $\sim 10^3$ yr, trace current SF. X-ray binaries, in which X-ray emission results from mass accretion onto a compact stellar remnant (NS or BH) from a main-sequence donor, are of the high-mass (HMXB) type or the low-mass (LMXB) type according to whether the donor mass is $M \gtrsim 8\ M_\odot$ or $M \lesssim 1\ M_\odot$ (see Persic & Rephaeli 2002, and references therein). HMXBs and LMXBs therefore trace, respectively, the current or average past SFR. The accreting object in ULXs is presumed to be a stellar (super-stellar) mass BH, accreting at super- (sub-) Eddington rates. Association with intense SF activity suggests that most ULXs are of the HMXB type (e.g., Zezas et al. 2002) – their optical counterparts having sometimes been positively identified as O stars (e.g., Liu et al. 2002). When observed in E/S0 galaxies (only occasionally, and limited to $L_{\rm x} \lesssim 2\times 10^{39}\ {\rm erg\,s^{-1}}$), ULXs are likely of the LMXB type (Sarazin et al. 2000; Kim & Fabbiano 2004). In both cases, ULXs appear to extrapolate X-ray binaries to higher accretor masses (e.g., Swartz et al. 2004).

The association of XPs with their host environment proves useful to measure XPLFs for uniform source population. Functions measured in starburst environments yield the young-XPLF, and XPLFs measured in "sterile" environments (e.g., in elliptical galaxies) reproduce the old-XPLF. As measured in systems with high SFR (e.g., in NGC 4038/9: Zezas & Fabbiano 2002; see discussion in Sect. 4.3), the differential young-XPLFs can be described by

$$\frac{{\rm d}N_{\rm y}}{{\rm d}L} = n_{\rm y,0}\,L^{-\beta_{\rm y}}, \quad \beta_{\rm y}\sim 1.5 \tag{1}$$

with the cumulative counts $N_{\rm y}(>L) \propto L^{-(\beta-1)}$. In the following we shall take Eq. (1) to represent the "universal" young-XPLF. The statistically superposed functions from a sample of E/S0 galaxies result in a completeness-corrected differential old-XPLF that is given by

$$\frac{{\rm d}N_{\rm v}}{{\rm d}L} = n_{\rm v,0}\times \begin{cases} L^{-\beta_{\rm v,1}} & L_1 \leq L < L_{\rm br} \\ L^{-\beta_{\rm v,2}} & L_{\rm br} \leq L \leq L_2 \end{cases} \tag{2}$$

with the faint-end slope and bright-end slope $\beta_{\rm v,1}\sim 1.8$ and $\beta_{\rm v,2}\sim 2.8$, the limiting luminosities $L_1 \sim 5\times 10^{37}\ {\rm erg\,s^{-1}}$ and $L_2 \sim 2\times 10^{39}\ {\rm erg\,s^{-1}}$, and the break luminosity $L_{\rm br} \sim 5\times 10^{38}\ {\rm erg\,s^{-1}}$ (Kim & Fabbiano 2004; see also Gilfanov 2004). The corresponding cumulative function has a low-L slope $\simeq 1$ and a high-L slope 1.8. In the following we shall take Eq. (2) to represent the "universal" old-XPLF (see discussion in Sect. 4.3). The break may highlight a change in the nature of the XP population: as its value approaches the Eddington limit for an accreting NS, the break may signal the NS to BH transition in the LMXB population.

Galaxies with mild ongoing SF, like our own Galaxy, have both young and old XPs. A direct separation of young and old XPs has been possible only in few cases (e.g., in M 81: Tennant et al. 2001). Usually, measured XPLFs reflect galaxy-integrated counts and hence result from a combination of young-XPLF and old-XPLF, whose relative normalization depends on the current to average-past SFR (see Grimm et al. 2003; Gilfanov 2004). Indeed, based on 1441 XPs detected in 32 nearby galaxies with different levels of SF activity, Colbert et al. (2004) concluded that XPs are linked to both the old and young stellar populations or, equivalently, to both the past and present SF activity (confirming the earlier suggestions of Fabbiano & Trinchieri 1985 and David et al. 1992). To estimate the current SFR, young XPs have to be culled from the total population.

3. Galaxy samples

Sample 1 (see Tables 1 and 2[1]) consists of local SFGs with available *IRAS* FIR fluxes, *ASCA*/*BeppoSAX*/*RossiXTE* 2−10 keV

[1] Additional information on sample 1 is reported in the following. (i) The values of the cumulative 2−10 keV XP luminosities, quoted in Table 1, result from converting the values measured in several different bands [0.3−10 keV for NGC 2403 (Schlegel & Pannuti 2003); 0.5−5 keV for NGC 6946 (Holt et al. 2003); 0.2−12 keV for IC 342 (Kong 2003); 0.5−8 keV for Arp 299 (Zezas et al. 2003); 2−8 keV for NGC 891 (Temple et al. 2005); 0.3−8 keV for NGC 4214 (Hartwell et al. 2004) and for all other objects (Colbert et al. 2004)] into the 2−10 keV band through an assumed photon spectrum $\phi \propto \epsilon^{-\alpha}$ [with $\alpha = 2$ in Kong (2003), 1.8 in Hartwell et al. (2004) and Temple et al. (2005), and 1.7 elsewhere]. In a few cases (NGC 4038/9, NGC 4449, NGC 5457, NGC 6946) it turns out that $\log L_{\rm XP} > \log L_{\rm x}$ (by $0.10 < \delta \log L \lesssim 0.30$): assuming such an unphysical situation to descend from non-optimal fits being performed on most XP spectra (except for those few XPs in each galaxy that had enough counts to allow detailed fits to be performed), in our computations we set $L_{\rm XP} = L_{\rm x}$. For NGC 4214 the XPLF slope is taken slightly steeper than quoted in Hartwell et al. (2004), to account for incompleteness that admittedly affects the XPLF shape below $\log L = 36.6$. For NGC 2403 the reported value of $L_{\rm XP}$ is

Table 1. Data Ia: local normal and starburst galaxies (SFG sample).

Object	D^a	$L_{\rm x}^b$	$L_{\rm XP}^c$	$L_{\rm min}$ | $L_{\rm max}^d$	γ^e	$B_{\rm T}^{0\,f}$	$f_{12\,\mu}^g$	$f_{25\,\mu}^g$	$f_{60\,\mu}^g$	$f_{100\,\mu}^g$	$f_{1.4}^h$
NGC 253	3.0	39.73	39.22	36.82, 38.42	0.75	7.09	41.04	154.67	967.81	1288.15	6.18
NGC 628	9.7	39.45	39.42	37.32, 38.42	1.11	9.76	2.45	2.87	21.54	54.45	0.173
NGC 891	9.6	40.32	39.57	37.42, 39.12	0.76	9.37	5.27	7.00	66.46	172.23	0.658
IC 342	3.9	40.30	40.02	37.44, 40.44	0.55	6.04	14.92	34.48	180.80	391.66	2.48
NGC 1569	1.6	37.83	37.72	35.82, 37.32	0.44	9.42	1.24	9.03	54.36	55.29	0.339
NGC 2146	17.2	40.59	40.44	37.85, 39.55	0.71	10.58	6.83	18.81	146.69	194.05	1.07
NGC 2403	4.2	39.29	38.45	36.02, 37.75	0.65	8.43	2.82	3.57	41.47	99.13	0.387
NGC 3034	5.2	40.70	39.82	37.32, 39.32	0.57	5.58	79.43	332.63	1480.42	1373.69	8.36
NGC 3077	2.1	37.91	37.58			10.24	0.76	1.88	15.90	26.53	
NGC 3079	20.4	40.59	39.69	37.62, 39.32	0.80	10.41	2.54	3.61	50.67	104.69	0.845
NGC 3628	7.7	39.84	39.32	36.82, 39.12	0.82	9.31	3.13	4.85	54.80	105.76	0.402
Arp 299	41.6	41.35	40.82	38.86, 40.26	0.50	11.85	3.97	24.51	113.05	111.42	0.977
NGC 4038/9	25.4	40.61	40.75	37.95, 39.95	0.63	10.62	1.94	6.54	45.16	87.09	
NGC 4214	3.48	38.68	38.65	36.36, 38.44	0.82	10.14	0.58	2.46	17.57	29.08	
NGC 4449	3.0	38.72	38.82	36.82, 38.22	0.70	9.94	2.1	4.7	36.0	73.0	0.600
NGC 4631	6.9	39.82	39.32	36.82, 39.02	0.69	8.61	5.16	8.97	85.40	160.08	1.12
NGC 4945	5.2	41.22	39.62	37.42, 38.92	0.70	7.43	27.74	42.34	625.46	1329.70	6.60
NGC 5236	4.7	40.09	39.62	37.32, 38.82	0.91	7.98	21.46	43.57	265.84	524.09	2.60
NGC 5457	5.4	39.38	39.62	36.82, 39.02	0.85	8.21	6.20	11.78	88.04	252.84	0.808
NGC 6946	5.5	39.64	39.66	36.76, 39.76	0.64	7.78	12.11	20.70	129.78	290.69	1.43

[a] Distances (in Mpc) are from Tully (1988) if $cz \leq 3000$ km s^{-1}, or consistently assume $H_0 = 75$ km s^{-1} Mpc^{-1} otherwise. [b] Integrated 2−10 keV luminosities (in erg s^{-1}; given in log form). For references see Persic et al. (2004a). For NGC 3077 and NGC 4214 see below. For NGC 4945 see Guainazzi et al. (2000). [c] Cumulative XP luminosities in the 2−10 keV band (in erg s^{-1}; in log form). [d] Minimum and maximum XP luminosities (in erg s^{-1}; given in log form), between which the XPLF index, γ, was derived. For spectral band information, see previous point. [e] Index of the cumulative XPLF, of the form $N(>L) \propto L^{-\gamma}$. For references, see point [c]. [f] Blue apparent magnitudes, corrected to face-on and for Galactic absorption, from RC3 (de Vaucouleurs et al. 1991). [g] *IRAS* flux densities at 12 μm, 25 μm, 60 μm, and 100 μm (in Jy), from Sanders et al. (2003; except for NGC 4449: Hunter et al. 1986). The FIR flux is accordingly defined (Helou et al. 1985) as $f_{\rm FIR} \equiv 1.26\times10^{-11}(2.58\, f_{60}+f_{100})$ erg s^{-1} cm^{-1}. [h] 1.4 GHz flux density (in Jy). No entry means that no data, or only upper limits to $f_{1.4}$, were found in the literature.

fluxes, and *Chandra* XPLFs. It spans ∼3 decades in SFR (estimated from $L_{\rm FIR}$, see Sect. 4), from levels typical of quiescent isolated spirals ($\lesssim 1\, M_\odot\,{\rm yr}^{-1}$) all the way up to strong merging starbursts ($\sim 50\, M_\odot\,{\rm yr}^{-1}$). As such, sample 1 is fairly representative of the range of SF activity in the local Universe.

based on the mean flux from its XPs (Schlegel & Pannuti 2003), excluding the 4 brightest sources and 12 presumed interlopers; the reported γ and η refer to the same set of sources represented by $L_{\rm XP}$ (see Sect. 6.1). For NGC 2146 the 2−10 keV XP data are taken from Inui et al. (2005). For NGC 3077 the luminosities of its 6 XPs and of the diffuse thermal plasma, measured in the 0.3−6 keV band (Ott et al. 2003), have been converted to 2−10 keV luminosities, using the individual published spectral models of Ott et al. (2003), and combined to give $L_{\rm x}$: the reported $L_{\rm XP}$ refers to the estimated young-XP luminosity; no published XPLF is available (see Sect. 6.1).

(ii) Radio data are from Kühr et al. 1981 (NGC 253), White & Becker 1992 (NGC 628, NGC 891, IC 342, NGC 2403, NGC 3034, NGC 3079, NGC 3628, Arp 299, NGC 4631, NGC 5457, NGC 6946), Condon et al. 1998 (NGC 1569, NGC 2146), Heeschen & Wade 1964 (NGC 4449), Wright & Otrupcek 1990 (NGC 4945, NGC 5236).

(iii) Compared with Persic et al. (2004a), several objects could not find their way into the present analysis. These systems and the reason for their exclusion are: NGC 55, NGC 891, NGC 1808, NGC 2276, NGC 5782, NGC 2903, NGC 3256[l], NGC 3310[l], NGC 3367, NGC 3556, NGC 4654, NGC 4666[l], NGC 7552: no published XPLF available ([l] observed with *Chandra* and/or *XMM-Newton*: Lira et al. 2002; Jenkins et al. 2004; Persic et al. 2004b); NGC 5253: no integrated 2−10 keV luminosity available (see Summers et al. 2004); NGC 7469, NGC 7679: AGN-dominated 2−10 keV emission.

(iv) Other commonly used names for some of the objects are: M 74 for NGC 628, M 82 for NGC 3034, NGC 3690 + IC 694 for Arp 299, Antennae for NGC 4038/9, M 83 for NGC 5236, and M 101 for NGC 5457.

Table 2. Data Ib: local normal and starburst galaxies (SFG sample).

Object	η^a	$L_{\rm FIR}^b$	$L_{\rm FIR}^{{\rm corr}\,c}$	SFR^d	$SFR^{{\rm corr}\,e}$
NGC 253	0.34	43.71	43.66	3.9	3.4
NGC 628	0.03	43.19	43.03	1.2	0.8
NGC 891	0.47	43.68	43.61	3.6	3.1
IC 342	0.95	43.29		1.5	
NGC 1569	1.00	41.88	41.76	0.06	0.04
NGC 2146	0.65	44.41	44.39	19.2	18.6
NGC 2403	0.33	42.74	42.37	0.41	0.17
NGC 3034	0.85	44.33	44.16	15.9	10.9
NGC 3077		41.65	41.48	0.03	0.02
NGC 3079	0.46	44.17	44.13	11.1	10.2
NGC 3628	0.29	43.34	43.24	1.7	1.3
Arp 299	0.96	45.02	45.02	78.9	77.9
NGC 4038/9	0.85	44.30	44.26	14.9	13.7
NGC 4214	0.19	42.13	41.96	0.10	0.07
NGC 4449	0.33	42.35	42.27	0.17	0.14
NGC 4631	0.53	43.44	43.30	2.0	1.5
NGC 4945	0.52	44.08	44.03	9.0	8.1
NGC 5236	0.15	43.61	43.54	3.0	2.6
NGC 5457	0.23	43.32	43.17	1.6	1.1
NGC 6946	0.73	43.46	43.27	2.1	1.4

[a] Derived 2−10 keV luminosity fraction of young XPs.
[b] Cirrus-uncorrected FIR luminosities (in erg s^{-1}), in log form.
[c] Cirrus-corrected FIR luminosities (in erg s^{-1}), in log form.
[d] Star formation rates, in $M_\odot$ yr^{-1}, uncorrected for cirrus emission. They are derived from IR luminosities using Eq. (3) and setting $L_{\rm IR} = 1.65 \times L_{\rm FIR}$.
[e] Star formation rates, in $M_\odot$ yr^{-1}, corrected for cirrus emission. They are derived as described in point [d].

Sample 2 (see Table 3) comprises a set of nearby Ultra-Luminous Infra-Red Galaxies (ULIRGs) with available *IRAS*

Table 3. Data II: starburst ULIRGs.

Source	z	D^a	f_x^b	L_x^c	$f_{12\mu}^d$	$f_{25\mu}^d$	$f_{60\mu}^d$	$f_{100\mu}^d$	$L_{\rm FIR}^e$	$L_{\rm IR}^f$	SFR^g	$f_{1.4}^h$	$L_{1.4}^i$
IRAS 12112+0305	0.072	293.0	−13.79	41.22	0.08	0.66	8.18	9.46	45.60	45.81	297		
IRAS 14348-1447	0.082	334.5	−13.72	41.41	0.07	0.55	6.82	7.31	45.62	45.84	315		
IRAS 15250+3609	0.055	222.9	−13.64	41.13	0.16	1.31	7.10	5.93	45.26	45.48	136	0.013	29.89
Arp 220	0.018	72.3	−12.74	41.06	0.61	8.00	104.0	112.0	45.48	45.69	225	0.30	30.27
IRAS 17208-0014	0.043	173.8	−13.34	41.22	0.20	1.61	9.53	11.05	45.21	45.43	122	0.10	30.56
IRAS 20100-4156	0.129	531.6	−13.65	41.88	0.1	0.57	5.44	5.41	45.90	46.12	595	0.02	30.83
IRAS 22491-1808	0.078	317.6	−14.19	40.89	0.06	0.54	5.54	4.64	45.46	45.68	216		

[a] Luminosity distances (in Mpc), computed from redshifts according to $D_{\rm L} = (2c/{\rm H}_0\Omega_0^2)\,[\Omega_0 z + (\Omega_0 - 2)(\sqrt{1+\Omega_0 z} - 1)]$ (Peacock 1999). [b] 2−10 keV fluxes (in erg cm^{-2} s^{-1} and given in log form), from Iwasawa et al. (2001) for Arp 220 and from Franceschini et al. (2003) for the remaining sources. [c] 2−10 keV luminosities (in erg s^{-1}), in log form. [d] *IRAS* flux densities (in Jy), from Genzel et al. (1998) and Sanders et al. (1995) for 20100-4156 and from Sanders et al. (2003) for the remaining sources. [e] FIR luminosities (in erg s^{-1}), in log form. [f] IR luminosities ($L_{\rm IR} \equiv 1.65 \times L_{\rm FIR}$; in erg s^{-1}), in log form. [g] Star formation rates (from Eq. (3)), in $M_\odot$ yr^{-1}. [h] 1.4 GHz flux densities (in Jy), from White & Becker (1992) for IRAS 15250+3609 and from Condon et al. (1996) for the remaining sources. [i] 1.4 GHz luminosities (in erg s^{-1} Hz^{-1}), in log form.

flux densities and *XMM* 2−10 keV fluxes. As suggested by their $L_{\rm FIR}$, these galaxies are sites of very intense star formation ($SFR > 100\,M_\odot\,{\rm yr}^{-1}$). Their 2−10 keV spectra show no evidence of AGN emission and are reminiscent, in their shapes, of Galactic HMXBs: this suggests that the entire $L_{\rm x}$ of these galaxies may be related to ongoing SF (see Franceschini et al. 2003). This set of starburst ULIRGs probes the peak of SF activity in the nearby Universe.

It is instructive to check the evolutionary stage of the SFGs represented in samples 1 and 2. As the spectral region ∼8−120 μm (sampled by the *IRAS* broad-band filters), which is characterized by continuum emission from hot dust, is very strongly affected by heating processes associated with SF, the *IRAS* color–color plot can be interpreted in terms of evolution of the SF activity. Based on advanced spectro-photometric modeling, Vega et al. (2005) suggested that the evolution of a starburst can be described as a sequence of four main phases (see Fig. 1): *(a)* an early-starburst phase, when the newly formed stars are still deep inside their placental clouds, and the escaping radiation field has not reached its peak emission; *(b)* a peak-starburst phase, when most massive stars are produced and are still embedded in their placental clouds, the SED is dominated by hot dust emission, and the starburst reaches its hottest colors; *(c)* an evolved-starburst phase, when the current SFR has decreased dramatically, the young hot stars have emerged from their progenitor clouds, and the cirrus emission is important; and *(d)* a post-starburst phase, when the current SF is mainly due to the quiescent disk and the colors are evolving towards those of normal spirals. According to this scheme, the location of our sample objects in Fig. 1 suggests that the ULIRGs are dominated by a starburst in its peak, while most local SFGs represent later phases, from evolved- through post-starburst to quiescent.

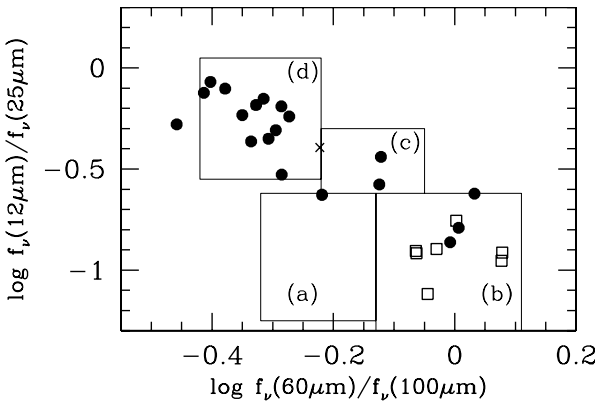

Fig. 1. *IRAS* color–color diagram of the galaxies of samples 1 (filled dots) and 2 (empty squares). Areas **a)** through **d)** denote successive phases of starburst evolution according to Vega et al. (2005; respectively: early-, peak-, evolved-, post-starburst).

4. FIR, radio galactic-SFR indicators

A significant fraction of the bolometric luminosity of an actively star-forming galaxy is absorbed by interstellar dust and reemitted in the FIR band. As the absorption cross-section of dust is strongly peaked in the UV, which inherently traces massive SF, the FIR emission can be a sensitive tracer of the current SFR. As discussed by Kennicutt (1998a,b), there probably is no single calibration that applies to all galaxy types. However, based on the main characteristics of our composite sample and guided by the general principle that the FIR emission should provide an excellent measure of the SFR in dusty starbursts, we shall adopt the most appropriate FIR SFR indicator for our current purposes.

A wide range of conversion relations between SFR and $L_{\rm FIR}$ are found in the literature, based on either a starburst model or an observational analysis (e.g., Hunter et al. 1986; Meurer et al. 1997; Kennicutt 1998a,b). Using the continuous-burst model of 10−100 Myr duration of Leitherer & Heckman (1995) and the Salpeter (1955) stellar initial mass function (IMF) with mass limits 0.1−100 $M_\odot$, Kennicutt (1998a,b) derived a conversion relation appropriate for starbursts:

$$SFR = \frac{L_{\rm IR}}{2.2\times10^{43}\,{\rm erg\,s^{-1}}}\,M_\odot\,{\rm yr}^{-1} \qquad (3)$$

with ∼30% uncertainty. Here $L_{\rm IR}$ refers to the full 8−1000 μm band: for starbursts with typical dust temperatures and emissivities, however, most of the emission falls in the FIR (∼40−120 μm) band, $L_{\rm FIR}/L_{\rm IR} \sim 0.6$ (Helou et al. 1988). Strictly speaking, the relation in Eq. (3) applies only to young starbursts embedded in optically thick dust clouds. In more quiescent SFGs the assumptions underlying the relation in Eq. (3) are not verified. Among these, the dust optical depth is lower, and a colder "cirrus" component, originating from the heating of the ISM by the galactic UV emission that is powered mostly by old stars, will contribute to the total FIR emission.

In this paper we adopt Kennicutt's conversion in Eq. (3) as a FIR-based SFR indicator. The insight on the evolutionary status of the galaxies in samples 1 and 2, discussed in Sect. 3, suggests some more accurate way of applying Eq. (3). As suggested by their FIR colors (see Fig. 1), all the ULIRGs of sample 2

and some of the SFGs of sample 1 are young, dusty, optically-thick starbursts that presumably meet the assumptions underlying Eq. (3) and hence can be straightforwardly treated with it, and their SFR can then be directly estimated from the observed $L_{\rm IR}$. For the remaining, milder SFGs of sample 1, which have evolved past the peak starburst phase, some of the assumption underlying Eq. (3) are not valid, so in principle their SFR cannot be directly estimated from the observed $L_{\rm IR}$. In particular, the FIR emission of these galaxies should be corrected for cirrus emission before being used as a SFR indicator. Since a detailed spectro-photometric modeling (e.g., Vega et al. 2005) of our sample galaxies is beyond our immediate scope, in this paper we follow David et al. (1992) in adopting Devereux & Eales's (1989) *statistical* cirrus correction. The basic assumption is that the strong empirical FIR-radio correlation holding for SFGs (Helou et al. 1985), interpreted as a consequence of massive SF (see below), is blurred by the SF-unrelated cirrus FIR emission, $L_{\rm FIR}^{\rm cir}$, most notably so at low luminosities, where in fact some nonlinearity occurs (see Condon 1992; Bell 2003). Setting $L_{\rm FIR}^{\rm cir} \propto L_{\rm B}$ (the blue luminosity being a proxy for the galactic stellar content), the SF-related FIR component is then $L_{\rm FIR}^{\rm SF} = L_{\rm FIR} - x\,L_{\rm B}$: the FIR-radio correlation is linearized and optimized if $x = 0.14$. The FIR luminosities in sample 1, although corrected according to this recipe for SFR-computing purposes, for simplicity will still be called $L_{\rm FIR}$ (see Table 2)[2]. Finally, the FIR ($\sim$40$-$120 μm) luminosities need a correction for the wider bandwidth ($\sim$8$-$1000 μm) required by Kennicutt's formula. Although such correction clearly depends on the detailed spectral energy distribution of each object, we here adopt a statistical correction and set

$$L_{\rm IR} = f \times L_{\rm FIR} \qquad f = 1.65 \tag{4}$$

to be used in Eq. (3). This bandwidth correction is, strictly speaking, valid for starbursts with $f_{60}/f_{100} = 1$ and dust emissivity index equal to 0 (Helou et al. 1988) and hence it may apply only to the ULIRGs of sample 2 and to some strong SFGs of sample 1; however, we assume that, after removal of the cirrus component, it is also sensible for the remaining, more mildly star-forming objects of Tables 1 and 2. In substantial agreement with our choice, Hopkins et al. (2003), Bell (2003), Kewley et al. (2002), and Calzetti et al. (2000) use a factor of 1.75 to convert from FIR to 1$-$1000 μm, the contribution to the 1$-$8 μm being in fact of the order of a few percent (see also Dale et al. 2001).

O stars are linked not only to the galactic thermal FIR emission through the heating of their placental clouds, but also to the galactic nonthermal radio emission through the acceleration of particles (which emit nonthermal synchrotron radiation) during their final SN explosion. This is reflected in a strong radio-FIR correlation, which can be quantified (Helou et al. 1985) by a parameter,

$$q_{\rm FIR} \equiv \log\left(\frac{f_{\rm FIR}}{\nu_{60\,\mu{\rm m}}}\right) - \log\left(f_{1.4\,{\rm GHz}}\right) \tag{5}$$

(with $f_{\rm FIR}$ in W m^{-2}, $\nu_{60\,\mu{\rm m}} = 3.75\times10^{12}$ Hz, and $f_{1.4\,{\rm GHz}}$ in W m^{-2} Hz^{-1}), that turns out to have a value

$$q_{\rm FIR} \simeq 2.35 \pm 0.02 \tag{6}$$

for local samples (Condon et al. 1991a; Yun et al. 2001; Bell 2003). In principle then, the nonthermal radio emission provides us with another sensitive tracer of the massive stellar population and hence of the instantaneous SFR (Condon 1992). For local SFGs, we adopt the calibration between 1.4 GHz luminosity and SFR,

$$SFR = \frac{L_{1.4}}{1.61\times10^{28}\,{\rm erg\,s^{-1}\,Hz^{-1}}} \tag{7}$$

derived by Schmitt et al. (2006) assuming a Salpeter stellar IMF with mass limits 0.1$-$100 $M_\odot$. Once adjusted for the same mass interval, this calibration produces SFRs a factor of $\sim$2 lower than the calibration of Condon (1992), which was based on the Galactic relation between nonthermal 1.4 GHz luminosity and SN rate; however, it is very similar to the more recent calibrations of Yun et al. (2001) and Bell (2003). (The above relations in Eqs. (3)$-$(7) are, of course, self-consistent.)

5. Analysis and results

To evaluate $L_{\rm x}^{\rm yXP}$, we model the measured XPLFs as linear combinations of the "universal" young and old XPLFs (see Eqs. (1) and (2)). The normalization ratio of the young to old differential XPLFs can be expressed as a function of the fractional young-XP luminosity, η, according to:

$$\frac{n_{\rm y,0}}{n_{\rm v,0}} = \frac{\eta}{1-\eta}\left[\frac{L_{\rm br}^{2-\beta_{\rm v,1}} - L_{\rm min}^{2-\beta_{\rm v,1}}}{2-\beta_{\rm v,1}} + \left(\frac{L_{\rm br}}{L_{\rm min}}\right)^{-\beta_{\rm v,1}} \times\frac{L_{\rm max}^{2-\beta_{\rm v,2}} - L_{\rm br}^{2-\beta_{\rm v,2}}}{2-\beta_{\rm v,2}}\right] \Bigg/ \left[\frac{L_{\rm max}^{2-\beta_{\rm y}} - L_{\rm min}^{2-\beta_{\rm y}}}{2-\beta_{\rm y}}\right]. \tag{8}$$

Since going back to the original XPLF data that are scattered in the literature is beyond the scope of the present work, in this paper we shall apply the young/old-XP decomposition to the published *fits* of the observed XPLFs. Only in the cases of NGC 628 and NGC 1569 did we choose to decompose the actual data. After performing random checks, we are confident that introducing this approximation has not biased the results of our modeling in any significant way. Our results are shown in Figs. 2 and 3.

One further step involves correcting $L_{\rm XP}$ for incompleteness of the corresponding XPLFs. In nearby galaxies the XPLFs can be measured down to $L_{\rm min} \sim 10^{36}$ erg s^{-1}, while in more distant galaxies the XPLFs can only be measured down to higher limiting luminosities, hence $L_{\rm XP}$ are biased low with distance. We correct for this bias – at least approximately – by assuming that all XPLFs can be extrapolated with the same γ down to $L_{\rm min} = 10^{36}$ erg s^{-1}. This leads to a new, distance-bias-corrected $L_{\rm XP}$. The flat XPLFs ($\gamma < 1$, except for NGC 628) ensure that these extrapolations are quite reasonable.

In Fig. 4-*top* the FIR-deduced SFRs are plotted versus $L_{\rm x}^{\rm yXP}$. The data clearly suggest a linear correlation,

$$SFR(>0.1\,M_\odot) = \frac{L_{\rm x}^{\rm yXP}}{0.75\times10^{39}\,{\rm erg\,s^{-1}}}\ M_\odot\,{\rm yr}^{-1} \tag{9}$$

(with a $\sim$20% statistical uncertainty on the calibration). Due to its normalization by a ratio of luminosities, the above relation is independent of the adopted cosmological model.

[2] For objects located at low Galactic latitudes ($|b| < 15$ degrees), the corrections for foreground Galactic absorption tend to be large and uncertain. An extreme case is IC 342 ($b = 10.58$ deg), for which the B-band absorption is estimated to be as large as 3.360 mag (Burstein & Heiles 1982) or 2.407 mag (Schlegel et al. 1998). As the adopted statistical correction for cirrus emission turns out to be unphysical in this case, we will drop IC 342 from further analyses. None of the results reported in this paper will depend on the exclusion of this object.

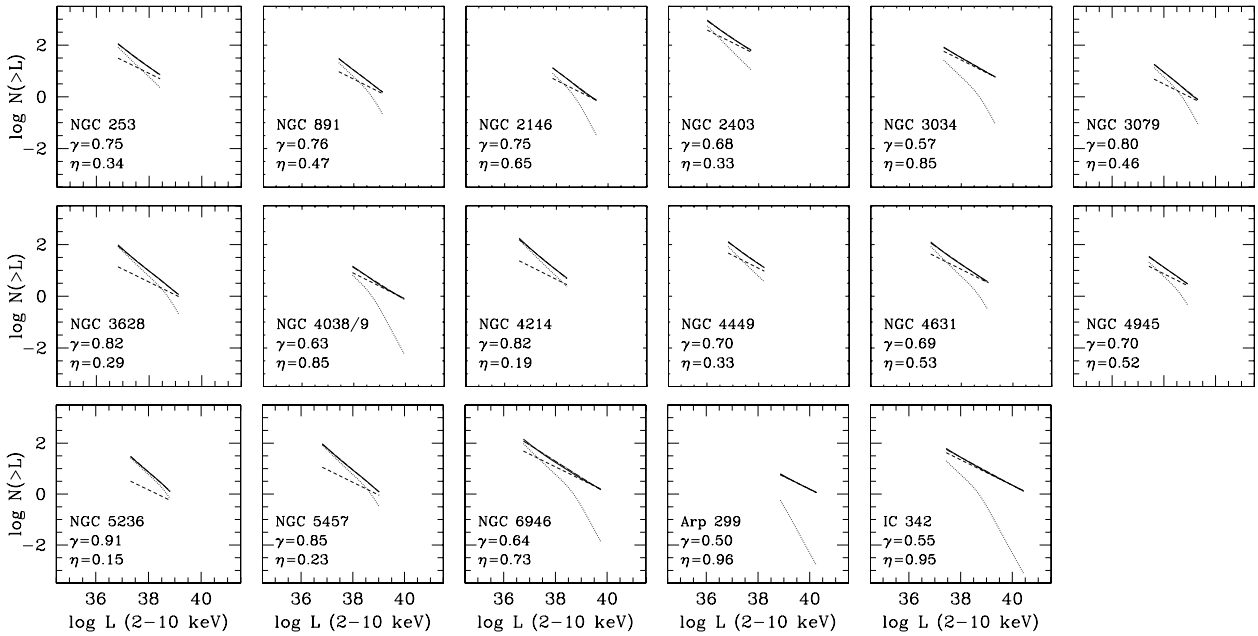

Fig. 2. Published fits to measured XPLFs (dot-dashed lines) are modeled as the sum (solid line) of a "young-XPLF" (dashed line; see Eq. (1)) and an "old-XPLF" (dotted line; see Eq. (2)). In each case, the cumulative old-XPLF component is normalized at the break luminosity, $L_{\rm br} = 5\times10^{38}$ erg s^{-1}, and its profile can be fitted with the following expression: $(1+x^{-1.02})/(1+x^{1.8})$ with $x = L/L_{\rm br}$.

6. Discussion

In this section we discuss some issues of relevance to the viability and use of $L_{\rm x}^{\rm yXP}$ as a SFR estimator. Specifically, we discuss properties of shape and calibration, and some underlying uncertainties, of the SFR–$L_{\rm x}^{\rm yXP}$ relation.

6.1. Linearity

Our SFR–$L_{\rm x}^{\rm yXP}$ relation appears to be linear over about 5 decades in luminosity and SFR. This result is consistent with that of Colbert et al. (2004), who, using a sample of 32 elliptical and spiral galaxies, found that $L_{\rm XP}$ was linear in both galaxy stellar mass and SFR (measured by K-band and FIR+UV luminosities, respectively). In our sample, however, poor statistics prevent a full assessment of the relation in the very-low-SFR regime.

In an attempt to gain furher insight, we examined the behavior of the very-low-SFR galaxy, NGC 3077, in the $L_{\rm x}^{\rm yXP}$–SFR plane. No published XPLF is available for this galaxy, but the measured spectra of its 6 detected XPs (Ott et al. 2003) can be used to single out young sources. The very soft sources S1, S5, and S6 are proposed by Ott et al. (2003) to be SNRs, and the hard source S3, speculated by Ott et al. (2003) to be an accreting binary, is spectrally consistent ($\Gamma \sim 1$) with being a HMXB. It was suggested by Ott et al. (2003) that S2 is an accreting binary or a background AGN: in the former case, its $\Gamma \sim 1.65$ slope may suggest a LMXB interpretation. The supersoft source S4 is argued by Ott et al. (2003) to be either a hydrogen-burning white dwarf or an isolated NS. If the identification of 4 young XPs is correct, then NGC 3077 approximately agrees with the SFR–$L_{\rm x}^{\rm yXP}$ relation defined for our composite sample (see Fig. 4-*top*).

NGC 2403 is another galaxy with very low SFR, potentially useful to investigate the low-L behavior of the SFR–$L_{\rm x}^{\rm yXP}$ relation. However, it seems to be a problematic object. As noted by Schlegel & Pannuti (2003) and discussed also by Fabbiano (2006), NGC 2403 is X-ray overluminous for its FIR luminosity and apparently violates Kilgard et al.'s (2002) correlation between XPLF-slope and FIR-based SFR. These apparent contradictions may be resolved assuming that SF in NGC 2403 turned off a few 10^6 yr ago: the FIR emission in the star-forming clouds, powered by OB stars, would be drastically reduced by now, whereas the HMXBs would still be shining (Schlegel & Pannuti 2003). We suggest an alternative possibility to reconcile NGC 2403's X-ray and FIR properties. Spectral modeling of the 4 brightest XPs of NGC 2403 (Schlegel & Pannuti 2003) suggests a LMXB nature for two of these (sources 1 and 28), and a BHXB nature for the other two (sources 20 and 21). For

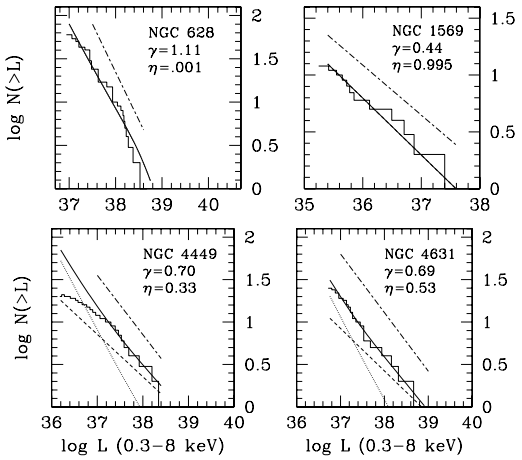

Fig. 3. The measured XPLFs of NGC 628 and NGC 1569 (histograms), not shown in Fig. 1, are modeled as the sum (solid line) of a "young-XPLF" (dashed line; see Eq. (1)) and an "old-XPLF" (dotted line; see Eq. (2)); their published power-law fits (see Table 1) are also shown, as arbitrarily shifted long/short-dashed lines. Similar information is displayed for NGC 4449 and NGC 4631 to exemplify our decomposition method on original XPLF data (as opposed to the corresponding published XPLF fits, shown in Fig. 1). In all cases, the power-law fits are displayed over the luminosity ranges where they were originally derived (see Table 1). NGC 4449 shows a clear case of incompleteness in source counts at low luminosities. All data are from Colbert et al. (2004).

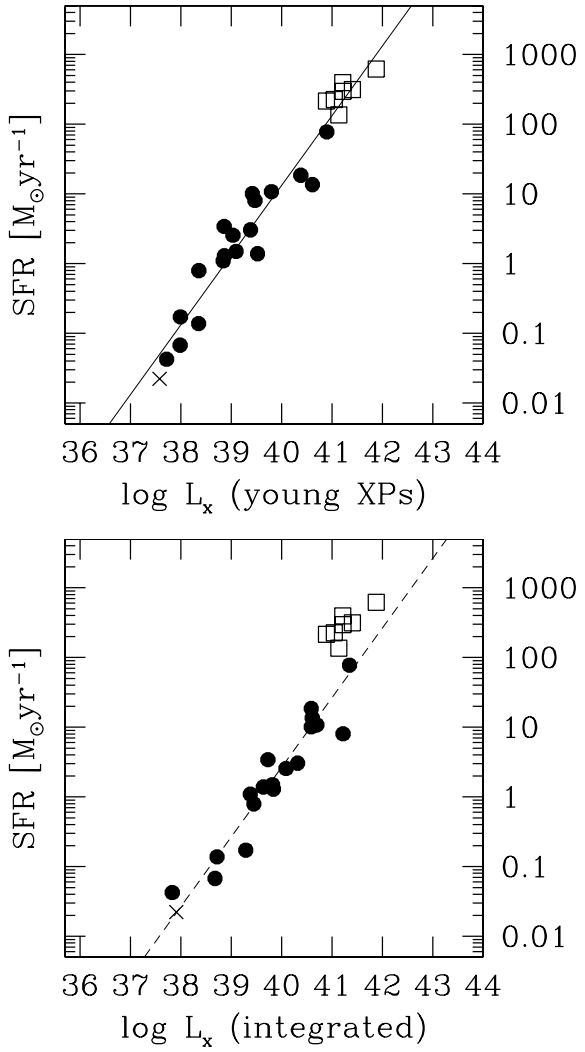

Fig. 4. The FIR-based SFR versus 2−10 keV luminosity relation, using the total luminosity (*bottom*) and the collective luminosity of young XPs (*top*) for the local sample of star-forming galaxies (filled circles: see Tables 1 and 2; NGC 3077 is represented by a cross) and the more distant sample of starburst ULIRGs (empty squares: see Table 3). In the latter set of high-SFR galaxies the emission is plausibly due to young XPs, hence the total 2−10 keV luminosities, $L_{\rm x}$, are used in both panels. The solid line in the *top* panel shows the relation in Eq. (9); the dashed line in the *bottom* panel shows the relation in Eq. (10).

the latter we also suggest a low-mass donor interpretation, based on the galaxy's very low SFR and the lack of spatial correlation with likely SF sites (see Schlegel & Pannuti 2003). If LMXB-related, the 4 brightest sources of NGC 2403 would no longer be unclassified and hence should be removed from the unclassified (as young or old) list of XPs. (Being old sources, these four sources would of course be unsuitable to trace the ongoing SF.) Of the remaining 37 less luminous unclassified XPs, distributed now in a truncated XPLF, 12 are estimated to be interlopers (apparently distributed randomly with luminosity, see Schlegel & Pannuti 2003). Finally, 25 sources are left as the galaxy's XP population out of which young sources have to be extracted by XPLF modeling. The young-XP luminosity estimated with our approach does comply with the SFR–$L_{\rm x}^{\rm yXP}$ relation (see Fig. 4-*top*). Further detailed study of NGC 2403 and its XP population is clearly much needed, both for its intrinsic interest, and for investigating the lowest-L reaches of the SFR–$L_{\rm x}^{\rm yXP}$ relation.

An analogous study of the use of young XPs (specifically: HMXBs) as SFR indicators led Grimm et al. (2003) to suggest a non-linear regime, SFR $\propto$ (luminosity)$^{0.6}$ for $SFR \lesssim 4.5\ M_\odot\ {\rm yr}^{-1}$, in the SFR–X-ray-luminosity relation. This behavior was attributed by Gilfanov et al. (2004b) to effects of low-numbers statistics in the distribution of XPs in low-$L_{\rm x}$, low-SFR galaxies. However, we suggest that differences in our sample selection and that of Grimm et al. (2003) may also play a role. The procedure of Grimm et al. (2003) involved a priori selection of galaxies with high SFR–to-stellar-mass ratios (based on dynamical estimates for the stellar masses of galaxies, and SFRs derived from a variety of indicators) to ensure that $L_{\rm x}$ would be HMXB-dominated and hence a tracer of the ongoing SFR. In contrast, we use all galaxies with measured source counts: by decomposing their XPLFs into young and old component, we a posteriori obtain the young-XP luminosity.

Given this uncertain situation, the faint limit of the SFR–$L_{\rm x}^{\rm yXP}$ relation clearly needs further investigation.

6.2. Calibration

The calibration of our SFR–$L_{\rm x}^{\rm yXP}$ relation, $(0.75 \pm 0.15) \times 10^{39}$ erg s^{-1} per $M_\odot$ yr^{-1}, is compatible with that, $\sim 10^{39}$ erg s^{-1} per $M_\odot$ yr^{-1}, derived by Grimm et al. (2003) using a variety of SFR estimators. Grimm et al. (2003) used $L_{\rm x}$ in their relation, but for their sample, which was selected such that $L_{\rm x}$ would be largely HMXB-dominated (see Sect. 6.1), $L_{\rm x} \sim L_{\rm x}^{\rm yXP}$ by construction.

Our calibration also agrees with the corresponding calibration of Colbert et al.'s (2004) bilinear correlation between $L_{\rm XP}$ and host-galaxy SFR and stellar mass. To see this we should account for the different definition of the variables, SFR and X-ray luminosity, in Colbert et al.'s (2004) Eq. (7) and in our Eqs. (3) and (4). Specifically, we convert their $L_{\rm FIR+UV}$-based definition of SFR into our adopted $L_{\rm IR}$-based definition, which gives $SFR_{\rm FIR+UV} = 1.067\ SFR_{\rm IR}$, and transform their 0.3−8 keV luminosities into our 2−10 keV luminosities (assuming with Colbert et al. (2004) $\Gamma = 1.7$ PL spectra), which gives $L_{0.3-8} = 1.529\ L_{2-10}$. In terms of our variables, Colbert et al.'s (2004) bivariate relation can be rewritten as

$$L_{\rm XP} - (0.85 \pm 0.13) \times 10^{29}\ M = (0.49 \pm 0.21) \times 10^{39}\ {\rm SFR}$$

(with 2−10 keV XP luminosities in erg s^{-1}, masses in $M_\odot$, and IR-derived SFR in $M_\odot$ yr^{-1}). Comparing this expression with Eq. (9) one sees that:

(i) our young-XP luminosity corresponds to Colbert et al.'s (2004) XP luminosity *minus* a quantity, proportional to the galaxy's stellar mass, that represents the old-XP luminosity: $L_{\rm x}^{\rm yXP} = L_{\rm XP} - (0.85 \pm 0.13) \times 10^{29} M$; and

(ii) once adjusted for the same definitions of SFR and luminosity, Colbert et al.'s (2004) calibration, $(0.49 \pm 0.21) \times 10^{39}$ erg s^{-1} per $M_\odot$ yr^{-1}, is consistent with ours.

6.3. Uncertainties

The main uncertainties concern the precision with which our adopted young-XPLF and old-XPLF have been detemined.

Old-XPLF. The old-XPLF proposed by Kim & Fabbiano (2004), though the most updated and reliable available, extends in luminosity down to only $\sim 5 \times 10^{37}$ erg s^{-1}, whereas measured

XPLFs often reach down to $\sim 10^{36}$ erg s^{-1}. In our analysis we chose to extrapolate Kim & Fabbiano's (2004) function down to $\sim 10^{36}$ erg s^{-1}, but this assumption may not be fully realistic. A flattening of the old-XPLF at $L \lesssim 10^{37}$ erg s^{-1}, with a differential slope of ~ 1, is suggested by counts of bulge LMXBs of some nearby spirals (Gilfanov 2004) and of XPs in NGC 5128 (Voss & Gilfanov 2006). However, the situation concerning the low-L XPLFs may be rather complicated. For example, in M 31's very well studied LMXB population clear differences are seen between bulge and globular-cluster XPLFs, and different low-L breaks appear in inner-bulge, outer-bulge, and globular-cluster XPLFs (see Fabbiano 2006, and references therein). Our choice is motivated by concerns of unexplored complexities in the low-L old-XPLF, as well as by the consideration that in SFGs the details of the low-L old-XPLF may not be crucial, if $L_{\rm XP}$ is dominated by bright sources – i.e., when the cumulative XPLF index is $\gamma < 1$, as is the case for the SFGs in Table 1 (except for NGC 628, whose measured XPLF however extends over a range where Kim & Fabbiano's (2004) function is defined).

In conclusion, use of Kim & Fabbiano's (2004) *combined* broken-PL old-XPLF probably represents a significant improvement in accuracy over the use of a single-PL with (cumulative) slope $\gtrsim 1$ as suggested by *individual* XPLFs (e.g., Kim & Fabbiano 2004; Colbert et al. 2004). We consider this assumption to be adequate for modeling XLPFs that do not extend much lower than $L \sim 10^{37}$ erg s^{-1}. But accurate modeling of deeper XLPFs (either measured or extrapolated) will require better knowledge of the low-L old-XPLF.

Young-XPLF. Either measured from very active global starburst galaxies (e.g., NGC 4038/9, Zezas & Fabbiano 2002) or from spatially resolved young XP population (e.g., M 81: Tennant et al. 2001; M 83: Soria & Wu 2003), young-XPLFs turn out as single PLs with (cumulative) slopes -0.5 ± 0.1 – the flatter slopes were measured in more intensely star-forming galaxies (Kilgard et al. 2002). Grimm et al. (2003) suggested the existence of a "universal" young-XPLF described as a single-PL, with cumulative slope -0.6 and normalization proportional to the SFR, in the luminosity interval $\sim 4 \times 10^{36}$–10^{40} erg s^{-1}. However, as discussed in Fabbiano (2006), a significant scatter of individual XPLF behaviors is observed. In our analysis we adopted Grimm et al.'s (2003) suggested regularity of a universal single-PL XPLF, but we chose the slightly flatter slope -0.5, which we feel (following Kilgard et al. 2002) to better represent homogeneous young-XP populations in high-SFR environments.

A further complication is possible. If in a high-SFR environment the stellar IMF is top-heavy (e.g., Doane & Mathews 1993; Rieke et al. 1993), the resulting correlation between SFR and stellar IMF implies a proportionally higher number of massive stars, and hence a flatter young-XPLF, for higher SFRs. This would in principle challenge the concept of a "universal" young-XPLF. If so, using the same young-XPLF to model the XPLFs of galaxies with very different SF activities would be incorrect and would lead to a systematic bias in the analysis. In this scenario, the assumption of a "universal" young-XPLF implies that SF sites in galaxies should have very similar characteristics everywhere within individual galaxies and in different galaxies, the main difference between high- and low-SFR galaxies being the number and sizes, not the physical properties, of such SF sites.

Given the known uncertainties, we checked that our main results are not significantly altered by changing our adopted young-XPLF slope by ± 0.1, which is believed to represent a reasonable uncertainty in the "universal" young-XPLF slope.

7. Star formation in the nearby Universe

To sample SF more completely in the nearby Universe, we extend our analysis to a sample of starburst ULIRGs[3]. Their very high SFRs ($\gtrsim 100\, M_\odot\, {\rm yr}^{-1}$), and the apparent flatness of their 2−10 keV spectra ($\Gamma \sim 1.2$: e.g., Franceschini et al. 2003) reminiscent of Galactic HMXB spectra, suggest that in these objects $L_{\rm x}$ mainly originate from young XPs. Then $L_{\rm x}^{\rm yXP} \sim L_{\rm x}$, and the current SFR of these galaxies is effectively traced by $L_{\rm x}$. Starburst ULIRGs are natural calibrators for the SFR–X-ray-luminosity relation. From Fig. 4-*top* we see that, using $L_{\rm x}$, our ULIRGs (empty squares) do lie on the extrapolation of the SFR-$L_{\rm x}^{\rm yXP}$ relation defined (at lower SFRs) by the SFG sample.

For a comparison with the SFR–$L_{\rm x}^{\rm yXP}$ relation in Eq. (9), we now consider the SFR–$L_{\rm x}$ correlation. For sample 1 this is reproduced by (see Fig. 4-*bottom*, filled circles):

$$SFR(>0.1\, M_\odot) = \frac{L_{\rm x}}{3.8 \times 10^{39}\, {\rm erg\, s^{-1}}}\ M_\odot\ {\rm yr}^{-1} \qquad (10)$$

(with a $\sim 20\%$ statistical uncertainty on the calibration). This expression is consistent with an analogous expression by Ranalli et al. (2003), based on nearly the same data, once their different definition of SFR, involving $L_{\rm FIR}$ instead of $L_{\rm IR}$, is accounted for. Inspecting the two relations in Fig. 4, it is clear that sample 1 complies with both, whereas sample 2 does not.

The mismatch between the SFG sample and the ULIRG sample in the SFR–$L_{\rm x}$ plane is so considerable that no simple function can adequately characterize our full combined sample over the SFR range ($-2 \lesssim \log[SFR/(M_\odot\ {\rm yr}^{-1})] \lesssim 2.5$) considered here. Since there is nothing special about the way our star-forming objects were selected, we suggest that the discrepancy is real and does not stem from a known bias. Our interpretation of the discrepancy is as follows. In all star-forming galaxies virtually the total $L_{\rm FIR}$ traces the istantaneous SFR, whereas $L_{\rm x}$, that is emitted partly by LMXBs (which represent the SFR of previous epochs) and partly by young sources (SNRs, HMXBs which trace the ongoing SFR), traces the integrated (from some previous epoch to the present) SFR. In those galaxies, therefore, only a fraction of $L_{\rm x}$ is related to the instantaneous SFR – a fraction which is large in SF-dominated galaxies (like our ULIRGs), but can be quite small in more quiescent spirals (e.g., the Galaxy) (see Fig. 5).

The simultaneous validity of both the SFR–$L_{\rm x}^{\rm yXP}$ and SFR–$L_{\rm x}$ relations for our local SFGs (with $SFR \leq 50\, M_\odot\, {\rm yr}^{-1}$) suggests that in these galaxies the SF activity has remained essentially constant over the past several 10^8 yr, so the corresponding SFR (traced by $L_{\rm x}$) is, for most galaxies of sample 1, approximately the same multiple of the instantaneous SFR (traced by $L_{\rm x}^{\rm yXP}$). It would be misleading, however, to infer the ratio of the integrated to instantaneous SFR from the normalization ratio (~ 5) of Eq. (10) to Eq. (9). We emphasize, in fact, that in sample 1 there is a systematic discrepancy between the XP luminosity (used to build $L_{\rm x}^{\rm yXP} \equiv \eta L_{\rm XP}$) and the integrated luminosity: $\langle L_{\rm XP}\rangle \simeq 0.40^{+0.11}_{-0.08}\langle L_{\rm x}\rangle$. This discrepancy may originate from inaccurate modeling of the individual XP spectra (affecting $L_{\rm XP}$; e.g., Schlegel & Pannuti 2003) and/or of the integrated galaxy spectra (affecting $L_{\rm x}$; e.g. Dahlem et al. 2000), or from the presence of a deeply buried AGN (e.g.: Della Ceca et al. 2002; Komossa et al. 2003; Ballo et al. 2004) or of truly diffuse

[3] By this definition we mean ULIRGs that show no obvious X-ray spectral evidence of harboring a central AGN (e.g., Franceschini et al. 2003).

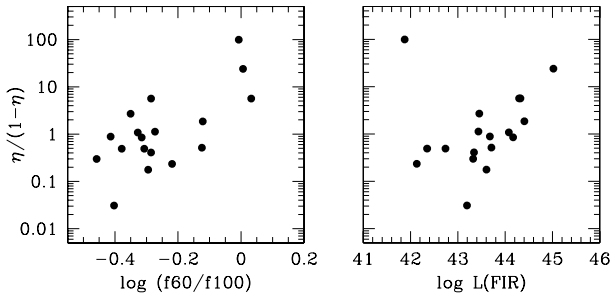

Fig. 5. The young- to old-XP 2−10 keV luminosity ratio plotted versus the temperature index f_{60}/f_{100} (*left*) and the FIR luminosity (*right*) for the galaxies in sample 1. The young-XP fraction is generally higher in more FIR-luminous galaxies, but the correlation appears to be tightest with the starburst phase (indicated by f_{60}/f_{100}): it is highest in peak-starbursts and gets progressively lower in evolved-starbursts and post-starbursts (see also Fig. 1). The outlier in the *right* panel is NGC 1569 whose *IRAS* colors are suggestive of a peak-starburst phase in spite of its low luminosity.

Table 4. Data III: *Hubble* Deep Field North galaxies.

Source	z	$f_{1.4}$	$L_{1.4}$	SFR	f_x	L_x
134	0.456	210	30.00	62.1/ 112.0	−15.55	41.13
136	1.219	180	30.87	455.5/ 821.3	−15.72	41.96
188	0.410	83	29.50	19.6/ 35.3	−16.24	40.34
194	1.275	60	30.43	167.8/ 302.5	−15.70	41.95
246	0.423	36	29.16	9.1/ 16.3	−16.12	40.49
278	0.232	160	29.26	11.3/ 20.4	−15.80	40.26

All fluxes (2−10 keV: erg cm^{-2} s^{-1}; 1.4 GHz: μJy) are rest-frame and are taken from Ranalli et al. (2003). Radio/X-ray luminosities (measured, respectively, in erg s^{-1} Hz^{-1} and erg s^{-1}), as well as X-ray fluxes, are given in log form. X-ray fluxes and luminosities were derived by modeling *Chandra* 0.5−8 keV counts with a power-law model (Ranalli et al. 2003). Star formation rates, derived from the 1.4 GHz luminosity by means of Eq. (7)/Eq. (11), are expressed in $M_\odot$ yr^{-1}.

emission (e.g., Griffith et al. 2000), or from a combination of all these. Whatever its origin, the discrepancy between L_x and L_{XP} contributes significantly to the difference between the normalizations of Eqs. (9) and (10). As a comparison, from Table 2 we derive $\langle\eta\rangle \simeq 0.50 \pm 0.07$ for sample 1. Hence $\langle L_x^{yXP}\rangle \sim 0.2\,\langle L_x\rangle$, as implied by the respective normalizations. (Incompleteness corrections, being relatively modest, do not substantially alter this result.)

8. Star formation at high redshift

Knowledge of the cosmological SF history is crucial to constrain models of galaxy evolution. One key step forward in this direction is developing our ability to measure the ongoing SFR in galaxies at cosmological distances, in a way that is mostly unaffected by absorption. Sample 3 is a set of distant ($z \sim 1$) *Hubble* Deep Field North galaxies (HDFNGs) with available 1.4 GHz flux densities and *Chandra*-based 2−10 keV fluxes (see Table 4). No FIR data are available. In Table 4 we report (from Ranalli et al. 2003) their (k-corrected: e.g., Bauer et al. 2002) rest-frame 2−10 keV luminosities and radio luminosity densities. The former are computed from *Chandra* counts in the soft (0.5−2 keV) and hard (2−8 keV) bands, assuming a power-law (PL) model. If a more realistic model is adopted, e.g., a sub-keV thermal plus a hard PL model (see Dahlem et al. 1998), the resulting 2−10 keV luminosities would be slightly (∼10%) lower.

The SFRs of our HDFNGs, estimated from $L_{1.4}$ using the (locally derived) conversion in Eq. (7), are high ($SFR \sim 100-1000\,M_\odot\,\mathrm{yr}^{-1}$: see Table 4), suggesting that these galaxies are SF-dominated (see also Cohen 2003). This, and the consideration that at the epoch corresponding to $z \sim 1$ (∼6 Gyr for our adopted cosmology) there had been no time for LMXBs to form, lead to the expectation that the L_x of our HDFNGs are largely dominated by young XPs. We then assume $L_x^{yXP} \sim L_x$. In the context of our current analysis, HDFNGs appear similar to ULIRGs.

The link between a starburst's instantaneous SFR and thermal FIR emission is well established, rendering L_{FIR} a relatively accurate estimator of the instantaneous SFR in starburst galaxies, most notably in their peak phase (see Sect. 4). This is not the case for the non-thermal radio emission, whose calibration with the SN rate is not known precisely (see Condon 1992; Condon et al. 2002) and whose characteristic synchrotron loss timescale strongly depends on the magnetic field – which can be very different in galaxies of, for example, very different SFR. This means that, in principle, in a given sample we should check the cross-correlation of the FIR-based and radio-based SFR indicators to ensure that the two sets of SFRs derived for that sample are mutually consistent. For a sample for which the radio SFR indicator is not known directly, combining the FIR SFR indicator in Eq. (3) with the observed FIR-radio correlation for that sample will yield a suitable radio-based SFR indicator.

Our direct knowledge of the FIR-radio correlation for deep samples is still quite limited. Garrett (2002), analyzing a sample of distant ($z \lesssim 1.3$) HDFNGs with $28.5 \lesssim \log[L_{1.4\,GHz}/(\mathrm{erg\,s^{-1}\,Hz^{-1}})] \lesssim 32$ (i.e., overlapping in luminosity with sample 2), could reach no conclusive results because the FIR fluxes of those galaxies, which were not directly accessible, had to be extrapolated from available *ISO* 15 μm data assuming a starburst template: the resulting q_{FIR} depended crucially on the adopted template, hence no information could be obtained on the actual value of q_{FIR} for that sample. Appleton et al. (2004), based on *Spitzer* 70 μm data for a distant galaxy sample in the luminosity range $10^{27} \lesssim L_{20\,cm}/(\mathrm{W\,Hz^{-1}}) \lesssim 10^{30}$ (i.e., overlapping in luminosity with sample 1), concluded that $q_{70} \simeq 2.15$ out to $z \sim 2$.

Attempting to circumvent any lack of direct knowledge, and pushing our assumption of similarity between HDFNGs and ULIRGs further, we *assume* that any FIR-radio correlation observed for the latter will also be representative of the former. Our own data suggest an ULIRG value of $q_{FIR} \simeq 2.6$ (Fig. 6-*top* [4]). The smallness of our ULIRG sample is somewhat compensated for by its homogeneity, as it includes only peak-phase starbursts (i.e., objects with $f_{60}/f_{100} \sim 1$). This is possibly the reason for the negligible scatter of our ULIRGs around $q_{FIR} = 2.6$ in Fig. 6-*top*. A likely confirmation comes from an analysis of Stanford et al.'s (2000) sample of high-z ULIRGs (with $29.5 \lesssim \log[L_{1.4\,GHz}/(\mathrm{erg\,s^{-1}\,Hz^{-1}})] \lesssim 31$, i.e., spanning the same luminosity range as our ULIRGs): although we find $2 \lesssim q_{FIR} \lesssim 2.6$, in agreement with Condon et al.'s (1991b) earlier result for a flux-limited *IRAS* sample of starbursts and ULIRGs, nevertheless, when obvious outliers and *IRAS* non-detections are removed, we find that most of Stanford et al.'s (2000) data are consistent with $q_{FIR} \sim 2.5-2.6$, definitely higher than the "canonical" local value of ∼2.35 (see Figs. 6-*middle*, 6-*bottom*).

[4] Also from Fig. 6, we point out that sample 1 has $q_{FIR} \sim 2.2$, hence it offers an essentially unbiased representation of the local SFG population.

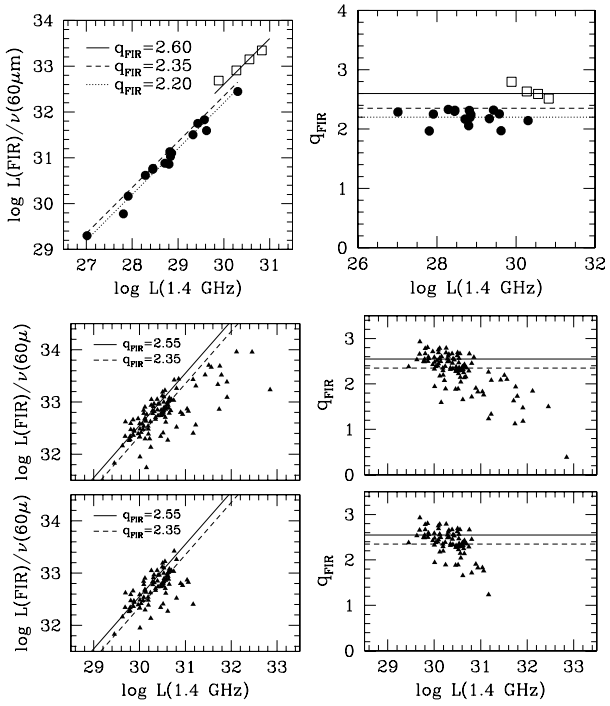

Fig. 6. The FIR-radio correlation (*left*) and, equivalently, the FIR/radio parameter $q_{\rm FIR}$ (*left*) for several samples of star-forming galaxies. *Top*: the local galaxies of sample 1 (filled circles, dotted line) and the relatively faraway ULIRGs of sample 2 (empty squares, solid line). The dashed line denotes the characteristic relation for local field galaxies according to Condon et al. (1991a), Yun et al. (2001), and Bell (2003). *Middle*: the high-redshift ULIRG sample of Stanford et al. (2000). All data are used; when 100 μm detections could not be obtained, 1σ upper limits were used to compute $L_{\rm FIR}$. *Bottom*: Stanford et al.'s (2000) sample, with non-detections and sources with $z > 0.45$ removed.

Based on the above considerations, we *tentatively* propose $q_{\rm FIR} = 2.6$ for the "pure starbursts" represented by the ULIRGs in sample 2. If, according to our assumption, this value is also representative of our HDFNGs, then by combining it with Eqs. (3)−(5) we obtain a consistent radio SFR indicator,

$$SFR = \frac{L_{1.4}}{8.93\times10^{27}\,{\rm erg\,s^{-1}\,Hz^{-1}}}, \qquad (11)$$

which we suggest may apply to ideal starbursts. The proposed conversion happens to be close to that of Condon (1992), who assumed a Galactic calibration of the non-thermal radio luminosity with SN rate, and to be higher by a factor of 1.8 than that of Schmitt et al.'s (2006). We shall use Eq. (11) alongside Eq. (7) to estimate SFRs from 1.4 GHz luminosities for our sample 3 galaxies.

Concerning the "nonthermal-luminosity versus SN-rate" calibration issue, we point out that Yun & Carilli (2002), using a FIR-radio spectral template in which the normalization of the non-thermal radio continuum had been left free to vary to determine a normalization most suitable for starburst galaxies, found that a local sample of FIR-luminous ($>10^{11}\ L_\odot$) galaxies were best fit by the Galactic normalization adopted by Condon (1992); and that the spectral template, incorporating such Galactic normalization, could fit the observed SEDs of some distant ($z\sim1$), intensely star-forming ($SFR\sim200-1000\ M_\odot\ {\rm yr}^{-1}$) galaxies. So Yun & Carilli's (2002) results may provide circumstantial evidence that in very high SFR environments, the calibration of the radio-SFR conversion may be quite similar to that adopted by Condon (1992) – and hence in implicit agreement with our proposed conversion in Eq. (11).

Using the data in Table 4, we plot the HDFNGs on the SFR versus X-ray luminosity plane (large filled triangles), for both $L_{\rm x}^{\rm yXP}$ (*top*) and $L_{\rm x}$ (*bottom*), in Fig. 7. The left panels use Schmitt et al.'s (2006) conversion in Eq. (7), whereas the middle panels use our proposed empirical conversion in Eq. (11). The right panels use Eq. (11) and a two-component (soft-thermal plus hard-PL) model, which are probably more realistic for starburst galaxies than Ranalli et al.'s (2003) simple PL model upon which the values of $L_{\rm x}$ in Table 4 are based. Inspection of Fig. 7 leads us to conclude that: *(a)* if Schmitt et al.'s (2006) local calibration also holds at high redshifts (or, alternatively, for strong starbursts), then our distant HDFNGs do not really seem to strictly follow either relationship, falling somewhere in between the two; *(b)* if our HDFNGs comply with Eq. (11), then they match the SFR–$L_{\rm x}^{\rm yXP}$ relation, but not the SFR–$L_{\rm x}$ relation; *(c)* the previous point is further strengthened if the HDFNG 0.5−10 keV spectra are similar to those of local starburst galaxies (e.g., Dahlem et al. 1998).

Therefore, the issue of where HDFNGs are located in the X-ray versus SFR plane is still unsettled. More investigations are needed to effectively measure the ongoing SFR in these galaxies. Broadband IR photometry would clearly prove crucial given the established role and effectiveness of the 8−1000 μm luminosity as a SFR indicator. Once calibrated – using IR-derived SFRs – on distant HDFNGs, the X-ray-based SFR indicator could be used to gauge ongoing SFRs in yet more distant galaxy samples.

9. X-ray versus radio SFR indicators

Finally, we plot all the galaxies of our combined samples on the X-ray versus radio luminosity plane (Fig. 8): the correlation involving $L_{\rm x}$ (*left*) is strong, whereas the one involving $L_{\rm x}^{\rm yXP}$ (*right*) is weak – a piecewise behavior is discernible, with a break at $L_{\rm x}^{\rm yXP}\sim5\times10^{39}\ {\rm erg\,s^{-1}}$. We interpret the different behavior as follows.

(a) The radio luminosity is a function both of the SN rate (hence the massive SFR) and of the average magnetic field strength. The syncrotron loss timescale is $\tau_{\rm s} = (\frac{4}{3}\frac{\sigma_{\rm T}}{m_{\rm e}c}\gamma_{\rm e}\frac{B_{\mu\rm G}^2}{8\pi})^{-1}\simeq 1.25\times10^{10}B_{\mu\rm G}^{-2}E_{\rm GeV}^{-1}$ yr, where $B_{\mu\rm G}$ is the magnetic field strength measured in μG, and $E_{\rm GeV}^2$ is the elecron kinetic energy measured in GeV. Assuming $E\sim5$ GeV (typical of electrons radiating at ∼1.4 GHz) and $B_{\mu\rm G}\sim1-5$ gives $\tau_{\rm s}\sim10^8-2.5\times10^9$ yr. Synchrotron loss timescales are then typically (much) longer than the typical SF timescale, $\tau_{\rm SF}\sim10^8$ yr. This means that the current radio emission of a local SFG may trace the SFR integrated over the last $\lesssim10^9$ yr. As remarked in Sect. 7, a similar consideration holds for the total 2−10 keV emission, $L_{\rm x}$.

(b) During a strong starburst phase we expect the prompt radio emission to be dramatically enhanced due to the more intense particle accleration (and perhaps also increased magnetic field, e.g., Hirashita & Hunt 2006), with a corresponding decrease in the synchrotron loss time. Clearly, the FIR energy density is much higher than (perhaps as high as $U_{\rm FIR}\sim10^{-8}\ {\rm erg\ cm^{-3}}$ in the starburst region; Condon et al. 1991b). Relativistic electron Compton energy losses are then important (with very short loss timescales, $\tau_{\rm IC} = (\frac{4}{3}\frac{\sigma_{\rm T}}{m_{\rm e}c}\gamma_{\rm e}\frac{U_{\rm FIR}}{10^{-8}{\rm erg\,cm^{-3}}})^{-1}\lesssim5\times10^4$ yr, for the same parameters as in the previous paragraph). Of course, Compton losses of

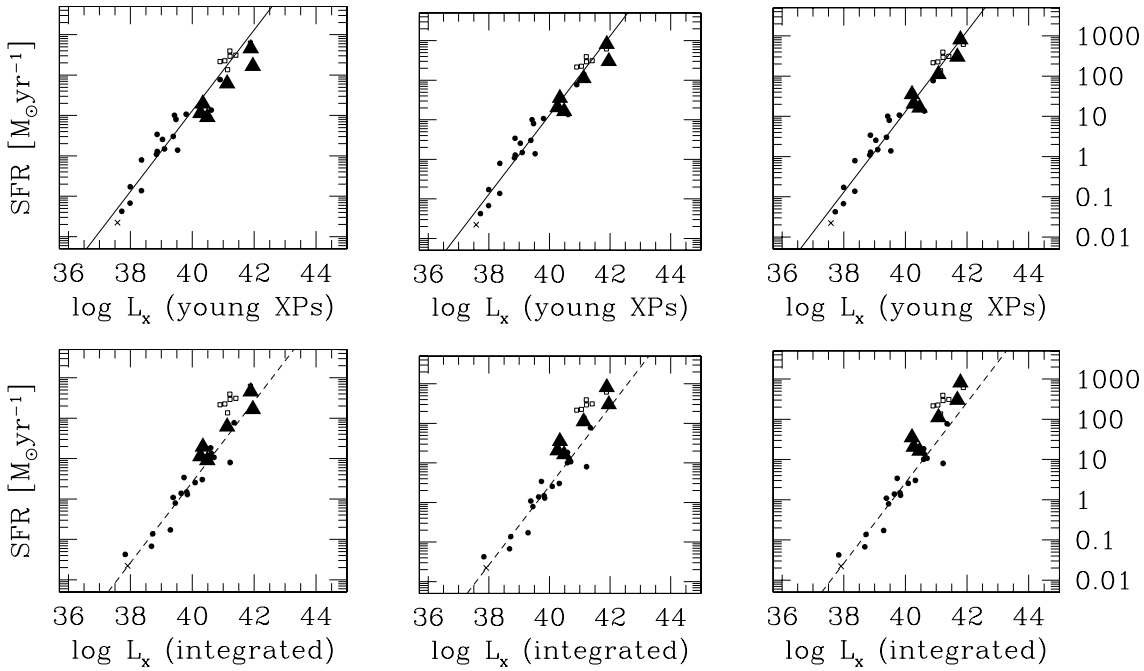

Fig. 7. The SFR versus 2−10 keV luminosity relations, using the collective luminosity of young XPs (*top*) and the total luminosity (*bottom*), for the distant sample of HDFNGs in sample 3 (large filled triangles) and, as a comparison, for the local SFGs in sample 1 (small filled circles) and the nearby ULIRGs in sample 2 (small empty squares). Because the emission of the HDFNGs is arguably due to young XPs, their total 2−10 keV luminosities, L_x, are used in both panels. These are computed from *Chandra* counts assuming a single-PL model (*left*, *middle*) and, alternatively, a soft-thermal plus hard-PL model (*right*). In the latter case, to maximize the effect we assumed the thermal component to have $0.2\,Z_\odot$ (e.g., Tsuru et al. 1997) and the PL component to have $\Gamma = 1.2$ (e.g., Franceschini et al. 2003). (All new luminosities were k-corrected accordingly.) HDFNG SFRs were computed from 1.4 GHz luminosity densities using Schmitt et al.'s (2006) locally-calibrated conversion in Eq. (7) (*left*) and our proposed "ideal starburst" conversion in Eq. (11) (*middle*, *right*). The relations in Eq. (9) (*top*, solid line) and in Eq. (10) (*bottom*, dashed line) are also shown.

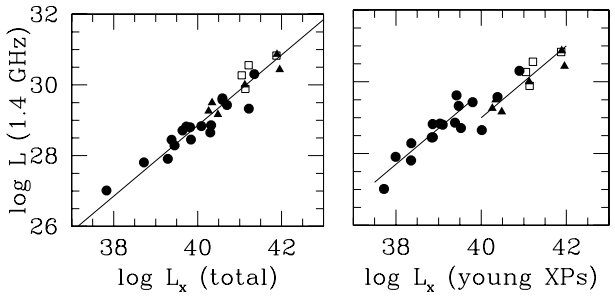

Fig. 8. 1.4 GHz luminosity densities are plotted versus 2−10 keV luminosities, using total luminosities (*left*) and collective young-XP luminosities (*right*), for the combined samples of local SFGs (filled circles), nearby ULIRGs (empty squares), and distant HDFNGs (filled triangles). The lines are solely meant to guide the eye.

synchro-emitting electrons off CMB photons increase with redshift as $(1 + z)^4$. These three factors (enhanced fresh radio emission and shorter synchrotron- and Compton-loss timescales) concur in making the observed radio emission of strong starbursts an accurate measure of their instantaneous SFR.

The varying ability of synchrotron radio emission to trace the instantaneous SFR, as a function of the different physical conditions prevailing in different galaxies, may play some role in the discussion on whether the value of $q_{\rm FIR}$ is "universal" and on the real meaning and calibration of the radio SFR indicator (see Sect. 8). In either case, the galactic radio and (total) X-ray luminosities should measure, at any given phase of a galaxy's SF history, essentially the same (definition of) SFR (i.e., instantaneous in strong starbursts, and integrated over the past $\lesssim 10^9$ yr in more quiescent disks). We thus expect a linear $L_{1.4\,\rm GHz}$–L_x correlation.

The integrated past SFR may in principle be unrelated to the current SFR, traced by $L_x^{\rm yXP}$. In our local SFGs galaxies, however, if the SF activity has remained essentially constant over the past several $\sim 10^8$ yr (as argued above), the past integral SFR traces (to a multiplicative factor) the current SFR. This makes the integrated vs. instantaneous SFR correlation possible, in the form of a linear correlation in the $L_{1.4\ \rm GHz}$, $L_x^{\rm yXP}$ plane (Fig. 8-*right*, filled circles). For strong starbursts a linear correlation exists, too, but it is displaced from the SFG one given the different definition of the SFR being measured by the radio emission in the two cases (instantaneous for starbursts, integrated for SFGs). Therefore the linear correlation between young-XP emission and radio emission would exist separately for mildly star-forming galaxies and for extreme starbursts. Its piecewise linearity, as well as the meaning of measuring the current versus integrated SFR, makes $L_x^{\rm yXP}$–$L_{1.4\ \rm GHz}$ a companion relation to SFR–L_x.

10. Summary and conclusion

In this paper we examined the issue of the collective 2−10 keV emission of young XPs and its role as a SFR indicator in star-forming galaxies. For a sample of local star-forming galaxies with available data, we estimated the young-XP luminosity by modeling the observed XPLFs in terms of "universal" young- and old-XPLFs. For $SFR \lesssim 50\,M_\odot\,{\rm yr}^{-1}$ galaxies, the collective emission of young XPs turns out to correlate linearly with the FIR-based SFR. In this SFR range both the SFR–$L_x^{\rm yXP}$ relation,

presented here, and the SFR–$L_{\rm x}$ relation, proposed by Ranalli et al. (2003), are valid. The relation is extended to higher SFRs by using a sample of extremely starburst-dominated ULIRGs. Since their $L_{\rm x}$ is arguably dominated by young XPs and hence by the instantaneous SFR, when $L_{\rm x}^{\rm yXP} = L_{\rm x}$ these ULIRGs comply with the SFR–$L_{\rm x}^{\rm yXP}$ relation. Similar considerations may hold for a sample of $z \sim 1$, intensely star-forming *Hubble* Deep Field North galaxies – especially so if their radio SFR indicator is calibrated slightly higher than for local galaxies, as suggested by the FIR-radio relation for starburst-dominated ULIRGs. Overall, the SFR–$L_{\rm x}^{\rm yXP}$ relation is suggested to hold over the broad SFR range $0.01 \lesssim SFR/(M_\odot\,{\rm yr}^{-1}) \lesssim 1000$, according to:

$$SFR(>0.1\,M_\odot) = \frac{L_{\rm x}^{\rm yXP}}{(0.75\pm0.15)\times10^{39}\,{\rm erg\,s^{-1}}}\ M_\odot\,{\rm yr}^{-1}.$$

For galaxies of very different SFRs, the same SFR–X-ray-relation holds only when the young-XP emission, *not* the total luminosity, is used. This is so because the FIR emission and the young-XP emission both trace the instantaneous SFR, whereas the total X-ray luminosity traces the instantaneous SFR in extreme starburst galaxies and the integrated SFR in more quiescent ones. Consequently, a SFR–$L_{\rm x}$ relation exists separately for very-low and very-high SFR galaxies (e.g., our local SFGs and distant ULIRGs, respectively). In particular, the existence of the SFR–$L_{\rm x}$ relation for our local, low-SFR galaxies suggests that SF has not changed dramatically over the last $\sim 10^9$ yr. The SFR–$L_{\rm x}^{\rm yXP}$ relation represents the most adequate X-ray estimator of the instantaneous SFR in galaxies. Its reflects the equivalence of two complementary measures of the current SFR, based on the observed manifestations of massive stars at their birth (short-lived FIR emission from placental dust clouds) and near their death as compact remnants (short-lived X-ray emission from close binary accretors), respectively.

Acknowledgements. This research has made use of the NASA/IPAC Extragalactic Database (NED), which is operated by the Jet Propulsion Lab, CalTech, under contract with NASA. We acknowledge constructive remarks from the anonymous referee and useful exchanges with several colleagues, including Ed Colbert, Pepi Fabbiano, Jimmy Irwin, Jean Swank, Rowan Temple, and Min Yun. This paper is fondly dedicated to the memory of MP's father, who died shortly before the inception of the work reported here.

References

Appleton, P. N., Fadda, D. T., Marleau, F. R., et al. 2004, ApJS, 154, 147
Ballo, L., Braito, V., Della Ceca, R., et al. 2004, ApJ, 600, 634
Bauer, F. E., Alexander, D. M., Brandt, W. N., et al. 2002, AJ, 124, 2351
Bell, E. 2003, ApJ, 586, 794
Burstein, D., & Heiles, C. 1982, AJ, 87, 1165
Calzetti, D., Armus, L., Bohlin, R. C., et al. 2000, ApJ, 533, 682
Cohen, J. G. 2003, ApJ, 598, 288
Colbert, E. J. M., Heckman, T. M., Ptak, A. F., et al. 2004, ApJ, 602, 231
Condon, J. J. 1992, ARA&A, 30, 575
Condon, J. J., Anderson, M. L., & Helou, G. 1991a, ApJ, 376, 95
Condon, J. J., Huang, Z.-P., Yin, Q. F., & Thuan, T. X. 1991b, ApJ, 378, 65
Condon, J. J., Helou, G., Sanders, D. B., & Soifer, B. T. 1996, ApJS, 103, 81
Condon, J. J., Cotton, W. D., Greisen, E. W., et al. 1998, AJ, 115, 1693
Condon, J. J., Cotton, W. D., & Broderick, J. J. 2002, AJ, 124, 675
Dahlem, M., Parmar, A., Oosterbroek, T., et al. 2000, ApJ, 538, 555
Dahlem, M., Weaver, K. A., & Heckman, T. M. 1998, ApJS, 118, 401
Dale, D. A., Helou, G., Contursi, A., et al. 2001, ApJ, 549, 215
David, L. P., Jones, C., & Forman, W. 1992, ApJ, 338, 82
de Vaucouleurs, G., de Vaucouleurs, A., Corwin, H. G. Jr., et al. 1991, The Third Reference Catalogue of Bright Galaxies, Univ. Texas Press, Austin (RC3)
Della Ceca, R., Ballo, L., Tavecchio, F., et al. 2002, ApJ, 581, L9
Devereux, N. A., & Eales, S. A. 1989, ApJ, 340, 708
Doane, J. S., & Mathews, W. G. 1993, ApJ, 419, 573
Fabbiano, G. 2006, ARA&A, ARA&A, 44, 323
Fabbiano, G., & Trinchieri, G. 1985, ApJ, 296, 430
Franceschini, A., Braito, V., Persic, M., et al. 2003, MNRAS, 343, 1181
Garrett, M. A. 2002, A&A, 384, L19
Genzel, R., Lutz, D., & Sturn, E., et al. 1998, ApJ, 498, 579
Gilfanov, M. 2004, MNRAS, 349, 146
Gilfanov, M., Grimm, H.-J., & Sunyaev, R. 2004a, MNRAS, 347, L57
Gilfanov, M., Grimm, H.-J., & Sunyaev, R. 2004b, MNRAS, 351, 1365
Griffiths, R. E., Ptak, A., Feigelson, E. D., et al. 2000, Science, 250, 1325
Grimm, H.-J., Gilfanov, M., & Sunyaev, R. 2003, MNRAS, 339, 793
Guainazzi, M., Matt, G., Brandt, W. N., et al. 2000, A&A, 356, 463
Hartwell, J. M., Stevens, I. R., Strickland, D. K., et al. 2004, MNRAS, 348, 406
Helou, G., Khan, I. R., Malek, L., & Boehmer, L. 1988, ApJS, 68, 151
Helou, G., Soifer, B. T., & Rowan-Robinson, M. 1985, ApJ, 298, L7
Heeschen, D. S., & Wade, C. M. 1964, AJ, 69, 277
Hirashita, H., & Hunt, L. K. 2006, A&A, 460, 67
Holt, S. S., Schlegel, E. M., Hwang, U., & Petre, R. 2003, ApJ, 588, 792
Hopkins, A. M., Miller, C. J., Nichol, R. C., et al. 2003, ApJ, 599, 971
Hunter, D. A., Gillett, V. C., Gallagher, III J. S., et al. 1986, ApJ, 303, 171
Inui, T., Matsumoto, H., Tsuru, T. G., et al. 2005, PASJ, 57, 135
Iwasawa, K., Matt, G., Guainazzi, M., & Fabian, A. C. 2001, MNRAS, 326, 894
Jenkins, L. P., Roberts, T. P., Ward, M. J., & Zezas, A. 2004, MNRAS, 352, 1335
Kennicutt, R. C. Jr. 1998a, ApJ, 498, 541
Kennicutt, R. C. Jr. 1998b, ARA&A, 36, 189
Kewley, L. J., Geller, M. J., Jansen, R. A., & Dopita, M. A. 2002, AJ, 124, 3135
Kilgard, R. E., Kaaret, P., Krauss, M. I., et al. 2002, ApJ, 573, 138
Kim, D.-W., & Fabbiano, G. 2004, ApJ, 611, 846
Komossa, S., Burwitz, V., Hasinger, G., et al. 2003, ApJ, 582, L15
Kong, A. K. H. 2003, MNRAS, 346, 265
Kühr, H., Witzel, A., Pauliny-Toth, I. I. K., & Nauber, U. 1981, A&AS, 45, 367
Lira, P., Ward, M., Zezas, A., et al. 2002, MNRAS, 330, 259
Liu, J.-F., Bregman, J. N., & Seitzer, P. 2002, ApJ, 580, L31
Ott, J., Martin, C. L., & Walter, F. 2003, ApJ, 594, 776
Peacock, J. A. 1999, Cosmological Physics (Cambridge: Cambridge University Press)
Persic, M., & Rephaeli, Y. 2002, A&A, 382, 843
Persic, M., Rephaeli, Y., Braito, V., et al. 2004a, A&A, 419, 849
Persic, M., Cappi, M., Rephaeli, Y., et al. 2004b, A&A, 427, 35
Ranalli, P., Comastri, A., & Setti, G. 2003, A&A, 399, 39
Rephaeli, Y., Gruber, D., Persic, M., & McDonald, D. 1991, ApJ, 380, L59
Rephaeli, Y., Gruber, D., & Persic, M. 1995, A&A, 300, 91
Rieke, G. H., Loken, K., Rieke, M. J., & Tamblyn, P. 1993, ApJ, 412, 99
Salpeter, E. E. 1955, ApJ, 121, 161
Sanders, D. B., Egami, E., Lipari, S., et al. 1995, AJ, 110, 1993
Sanders, D. B., Mazzarella, J. M., Kim, D.-C., et al. 2003, AJ, 126, 1607
Sanders, D. B., Scoville, N. Z., & Soifer, B. T. 1991, ApJ, 370, 158
Sarazin, C. L., Irwin, J. A., & Bregman, J. N. 2000, ApJ, 544, L101
Schlegel, D., Finkbeirer, D. P., & Davis M. 1998, ApJ, 500, 525
Schlegel, E. M., & Pannuti, T. G. 2003, AJ, 125, 3025
Schmitt, H. R., Calzetti, D., Armus, L., et al. 2006, ApJ, 643, 173
Soria, R., & Wu, K. 2003, A&A, 410, 53
Stanford, S. A., Stern, D., van Breugel, W., & De Breuck, C. 2000, ApJS, 131, 185
Summers, L. K., Stevens, I. R., Strickland, D. K., & Heckman, T. M. 2004, MNRAS, 351, 1
Swartz, D. A., Ghosh, K. K., Tennant, A. F., & Wu, K. 2004, ApJS, 154, 519
Temple, R., Raychaudhury, R., & Stevens, I. 2005, MNRAS, 362, 581
Tennant, A. F., Wu, K., Ghosh, K. K., et al. 2001, ApJ, 549, L43
Tsuru, T. G., Awaki, H., Koyama, K., & Ptak, A. 1997, PASJ, 49, 619
Tully, R. B. 1988, Nearby Galaxies Catalog (Cambridge: Cambridge Univ. Press)
Vega, O., Silva, L., Panuzzo, P., et al. 2005, MNRAS, 364, 1286
Voss, R., & Gilfanov, M. 2006, A&A, 447, 71
White, R. L., & Becker, R. H. 1992, ApJS, 79, 331
Wright, A., & Otrupcek, R. 1990, Parkes Catalogue, Australia Telescope National Facility
Yun, M. S., & Carilli, C. L. 2002, ApJ, 568, 88
Yun, M. S., Reddy, N. S., & Condon, J. J. 2001, ApJ, 554, 803
Zezas, A., & Fabbiano, G. 2002, ApJ, 577, 726
Zezas, A., Fabbiano, G., Rots, A. H., & Murray, S. S. 2002, ApJ, 577, 710
Zezas, A., Ward, M. J., & Murray, S. S. 2003, ApJ, 594, L31